

## Experimental characterisation of the waves propagating against current effects on the wake of a wide bathymetric obstacle

Y. SAOULI<sup>(1)</sup>, M. MAGNIER<sup>(1,2)</sup>, G. GERMAIN<sup>(1)</sup>,  
B. GAURIER<sup>(1)</sup>, P. DRUAULT<sup>(2)</sup>  
*mmagnier@ifremer.fr ; ysaouli@ifremer.fr ; ggermain@ifremer.fr;*

<sup>(1)</sup>Laboratoire Hydrodynamique Marine, Ifremer, Boulogne-sur-Mer

<sup>(2)</sup>Institut Jean Le Rond d'Alembert, Sorbonne Université, CNRS, Paris

### Summary

The upcoming development of tidal turbine farms requires a great understanding of the environment in which they will be installed. The aim of this study is to better understand the effects of surface waves on the high-energy turbulence generated by the interaction between tidal currents and the bathymetry. To do so, specific conditions are reproduced in the IFREMER's flume tank at Boulogne-sur-Mer. The bathymetry is represented by a square-based cylinder mounted on the tank floor perpendicularly to the current, in Froude similarity, at a scale of 1:20. The chosen wave conditions make it possible to study the wave frequency and wave amplitude effects on the obstacle wake development. From PIV measurements, the results show that, for a current speed of 0.8 m/s, low frequency waves ( $Tp > 13$  s at sea) are the most impactful. When the frequency is high, the surface wave amplitude must be greater ( $H_s > 3$  m at sea) to modify the vortex shedding behind the obstacle. Whenever the cylinder wake is altered by the waves, the wake goes faster towards the surface. The vortex shedding, already present without waves, becomes more energetic and focuses on a sub-harmonic of the wave frequency.

### I – Introduction

In high-potential tidal turbine sites, the strong tidal currents are interacting with the local bathymetry, creating a vertical velocity gradient and turbulent structures. Furthermore, in those sites, surface gravity waves are often present as well, especially in winter [3]. Turbulent and shear tidal currents interact with surface waves which creates complex hydrodynamic conditions, both spatially and temporally. The behaviour of the tidal flow is thus modified: mean velocity profiles and turbulent characteristics are altered by the wave motions, as the wave kinematics are changed by the current [12].

Many studies have been conducted in coastal-like conditions. [9] and [1] show that the wake of wall-mounted obstacles is modified by the presence of surface waves which in return are modified as well by the presence of those obstacles. [10] shows that surface waves with the current decrease the intermittency of the current turbulence and modulate the energy cascade. A year later, [11] states that high frequency waves inhibit the small-scale fluctuations and enhance the medium scale fluctuations in the stream-wise direction more strongly than lower frequency waves. The properties of flow variabilities are thus strongly modified in coastal area.

In this study, the goal is to understand how the surface waves modify the velocity variations in a tidal energy site. To do so, a wide bottom-mounted cylinder set perpendicularly to the flow is used to generate bathymetry-current energetic turbulence. The experiment is scaled to be in Froude similarity to the Alderney Race. Then, surface waves propagating against the current are generated and the square cylinder wake is compared with its wake without waves, as presented in [5]. Our study follows the same methodology than in [7], in which it is determined that for waves propagating with the current, the low frequency waves have the most impact on the cylinder wake.

In this paper, an experimental investigation of the interaction between waves against tidal current and a wide bottom-mounted obstacle is carried out to complete the results previously obtained. The experimental set-up and flow characteristics are presented first. Then velocity, turbulent kinetic energy and Reynolds shear stress are studied. Finally, a spectral analysis is done to highlight how waves modify the vortex shedding in the cylinder wake.

## II – Experimental set-up and input characteristics

### II – 1 Sea conditions modelling in the flume tank

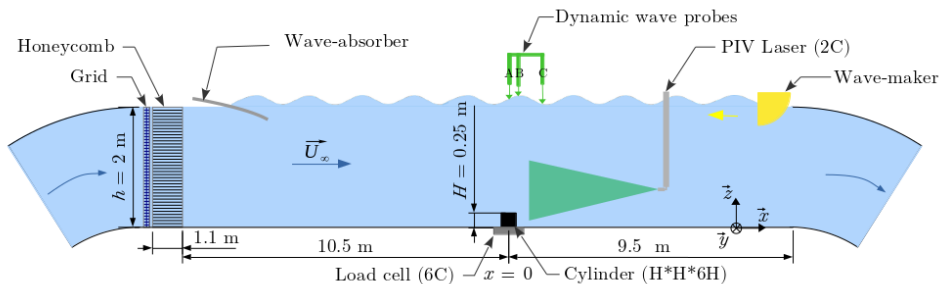


Figure 1: Flow configuration sketch showing the cylinder and the 3 wave gauges locations, the PIV laser sheet, and the wave-maker at the outlet of the test section. The current flows from left to right and the waves propagate from right to left.

Tests are carried out in the wave and current circulating tank of IFREMER in Boulogne-sur-Mer (France). The test section is 20 m long  $\times$  4 m wide  $\times$  2 m deep (see Fig. 1). The incoming flow ( $U_\infty, V_\infty, W_\infty$ ) is assumed to be constant and steady, with the imposed velocity:  $U_\infty = 0.8$  m/s and  $V_\infty = W_\infty = 0$  m/s. The three instantaneous velocity components are denoted ( $U, V, W$ ) along the ( $x, y, z$ ) direction respectively. According to the Reynolds decomposition, each instantaneous velocity component is separated into a mean value and a fluctuating part:  $U = \bar{U} + u'$  where the over-bar indicates the time average. Thanks to a grid combined with a honeycomb placed at the inlet of the working

	Scale	$U_\infty$ [m/s]	Rugosity $H$ [m]	Depth $h$ [m]	$Re_H$ [-]	$Fr$ [-]
Alderney Race	1	3.5	5	40	$1.8 \times 10^7$	0.18
Flume tank	1/20	0.8	0.25	2	$2.0 \times 10^5$	0.18

Table 1: In-situ and experimental conditions (1:20 scale).

section, a low turbulence intensity  $I_\infty = 1.5\%$  is reached [5] and the boundary layer height, calculated as follows:  $\delta_{95} = z(\bar{U} = 0.95 \times U_\infty)$ , is equal to  $\delta_{95} \approx 0.25$  m.

To represent at scale a large seabed roughness, a square cylinder of section  $H \times H$ , with  $H = 0.25$  m, and of width  $6H$  is used (see Fig. 2 middle and right) [8]. The  $x$ -origin is set at the centre of the cylinder and  $z = 0$  corresponds to the tank floor. The cylinder is centred in the span-wise direction of the tank. Span-wise origin ( $y = 0$ ) is set to the centre of the cylinder, and thus of the tank (Fig. 1).

For the present investigation, the Reynolds number of the incoming flow is  $Re_H = HU_\infty/\nu = 2.0 \times 10^5$  with  $\nu$  the water kinematic viscosity. The Froude number is equal to  $Fr = U_\infty/\sqrt{g \times h} = 0.18$ , with  $h$  the flume tank depth and  $g$  the gravity. The scaled experiment has then dimensionless parameters similar to those of real sea conditions [5], for which the Alderney Race conditions (a potential tidal site in French water) have been considered. These parameters are presented in Table 1.

To generate waves at the flume tank surface, a wave generator is used. In this experiment, it is set at the outlet of the working section of the tank, as shown in Fig. 1 and Fig. 2 (left). At the inlet of the working section, a wave-absorber (a damping beach), made of a metallic porous panel (8% porosity), is set to reduce as much as possible wave reflection on the outlet wall of the tank. The wave cases studied here are shown in Table 2 (right).

In this study, four cases, named  $f0 \square 0L$ , have the same wave amplitude ( $\overline{A_{O1}} \approx 2.5$  cm) and frequencies from 0.203 Hz to 0.500 Hz. Three cases, named  $f040 \square$ , have the same wave frequency equal to  $f_h = 0.406$  Hz but different wave amplitudes. This enables to study both the effects of the wave amplitude and of the wave frequency. Furthermore, according to [4], the average significant wave height  $H_s$  is 1.3 m in the Alderney Race, and the most common  $H_s$  is between 0.4 m and 1 m. All of these events come from the west with peak period  $T_p$  between 10 s and 16 s. As shown in Fig. 3, the flume tank conditions represent well the ones observed at sea at scale 1:20 using Froude similarity.

## II – 2 Measurement tools

To characterise the flow, Particle Image Velocimetry (PIV) measurements are conducted in the symmetry plane of the cylinder. To capture the entire cylinder wake, 3 planes are made along the  $x$ -axis. The measurements are made using the camera Hisense Zyla USB 5.5, with a greyscale coding parameter of 12 bits for each pixel. Measurement planes dimensions are 1.60 m  $\times$  1.12 m with a spatial resolution of  $dx = dz = 20$  mm. Fig. 2 (middle) presents their spatial organisation. Before PIV measurements, the tank is seeded with 10  $\mu$ m diameter silver coated glass micro-particles. Particles illuminated by a 200 mJ Nd-Yag laser are detected on 4 to 10 pixels. Adaptive PIV is used to calculate particle displacements between two images to obtain particles velocity, and outliers are

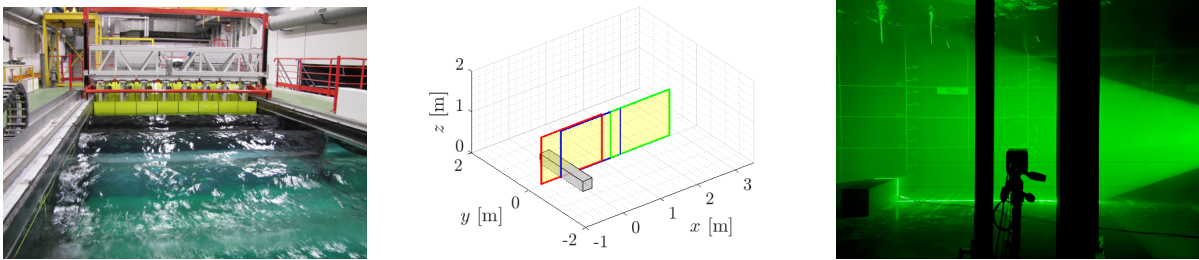


Figure 2: Left: Picture of regular waves in the Ifremer current flume tank. Centre: PIV plane configuration. Right: Picture of the PIV set-up with the camera in foreground and the laser sheet that illuminates the square cylinder. The resistive wave gauges are passing through the free surface where a wave trough is visible on top of the cylinder.

replaced with the Universal Outlier Detection method (with the software DynamicStudio from Dantec Dynamics). PIV acquisitions are made during 200 s, hence 3000 pairs of images are taken at 15 Hz acquisition frequency. The time between the images of a double-frame is  $\Delta t = 900 \mu\text{s}$ . For the data presented in section II – 3, the greyscale is encoded on 16 bits and the time between the two images of a double-frame is  $\Delta t = 8000 \mu\text{s}$ .

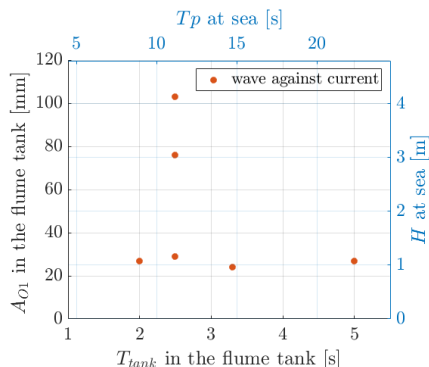
The surface elevation is also measured with a combination of KENEK servo-type wave probes (model SHT3-30E) and resistive wave probes. The dynamic wave probe (denoted  $A$  in Fig. 1) is set on top of the cylinder, at  $(x, y) = (0, 0)$  m. Two resistive probes are set downstream, on the positions  $B$  and  $C$  on the flume tank sketch, with  $AB = 52$  cm and  $BC = 70$  cm. Wave probe  $A$  is used to quantify the average wave height.  $B$  and  $C$  wave probes are used to calculate the wavelength of the generated waves.

Finally, the wave probes are synchronised to the PIV system that triggers the measurements. For each wave condition, the measurements are launched when the conditions are stationary.

## II – 3 Input waves and flow characterisation

In this experimental investigation, 6 regular wave conditions are studied. They are introduced in Table 2 and presented at sea scale in Fig. 3.  $f_h$  is the exact frequency at which waves are generated by the wave-maker, and their period is defined as  $T_{tank} = 1/f_h$ . The wave amplitude  $\overline{A_{O1}}$  corresponds to the time average wave amplitude at the wave frequency, calculated by taking the average of the Hilbert Transform of the surface elevation  $\eta_A$  (given by wave gauge  $A$ ) filtered around the wave frequency.  $\lambda$  is the wavelength calculated directly with the wave probes phase difference and the distance between the probes, except for the case  $f020L$  and  $f030L$  for which the wavelength is too long compared to the distance between the wave gauges  $A$  and  $C$  used for the calculation. For these two cases (emphasized by a \* in the Table), the wavelength is calculated using Airy wave theory modified by current from Brevik & Bjørn [2]. The standard deviation  $\sigma(A_{O1})$  of the Hilbert Transform of  $\eta_A$  is also calculated (not given here). For all wave cases,  $\sigma(A_{O1})$  represents less than 5% of  $\overline{A_{O1}}$ . For all cases, the first sub-harmonic appears in the spectrum of  $\eta_A$ . It represents less than 10% of  $\overline{A_{O1}}$  except for  $f030L$  ( $\overline{A_{O2}} = 21\%$ ) and  $f040H$  ( $\overline{A_{O2}} = 11\%$ ). In  $f030L$  case, this high level sub-harmonic is explained by its frequency  $\approx 0.6$  Hz, which corresponds to a characteristic mode of the flume tank linked to its dimensions. For  $f040H$ , this is explained by its high energy level due to the

high wave amplitude of this study-case. The wave energy flux is calculated as follows:  $J_s = \frac{\rho g^2}{64\pi} (2\overline{A_{O1}})^2 T_{tank}$ , and is especially high for the cases  $f020L$ ,  $f040M$  and  $f040H$ .



Case	$f_h$ [Hz]	$T_{tank}$ [s]	$\overline{A_{O1}}$ [cm]	$\lambda$ [m]	$J_s$ [ $\frac{W}{m}$ ]
$f020L$	0.203	4.92	2.7	16.3*	1273
$f030L$	0.297	3.37	2.4	9.1*	774
$f040L$	0.406	2.46	2.9	5.0	684
$f040M$	0.406	2.46	7.6	4.9	1792
$f040H$	0.406	2.46	10.3	4.9	2429
$f050L$	0.500	2.00	2.7	3.3	517

Figure 3: Wave cases in the tank and their equivalent at sea. As the waves are regular in the tank,  $H_s \approx H$ .

Table 2: Wave cases characteristics.  $f_h$ : wave frequency, with  $T_{tank} = 1/f_h$ .  $\overline{A_{O1}}$ : time average wave amplitude.  $\lambda$ : wavelength from measurements except for the \* cases.  $J_s$ : wave flux energy.

Figure 4 presents the mean stream-wise and vertical velocity profiles at  $(x, y) = (0, 0)$  m, compared to the velocity profile with the wave-maker and the wave-absorber set in the water (WM case) and out of the water (Ori. config, i.e. Original configuration of the flume tank).

In the bottom half of the flume tank, all velocity profiles have the same shape (boundary layer until  $z \approx 0.3$  m and almost constant upper), but then their values differ. This is explained by the wave-absorber presence at the inlet which slows down the flow near the surface, thus accelerating the flow in the bottom half of the tank to keep the same flow rate. The vertical velocity is not modified by adding the wave generator and absorber, nor than with waves compared to current-only:  $\overline{W}$  stays  $\approx 0$  m/s. Compared to the original configuration (current only), the addition of the wave absorber/generator and of waves is responsible for a slight increase in turbulent intensity in the bottom part of the tank. In the upper part of the water column, the presence of the wave-absorber generates a higher level of turbulence, as seen in Fig. 5 (left).

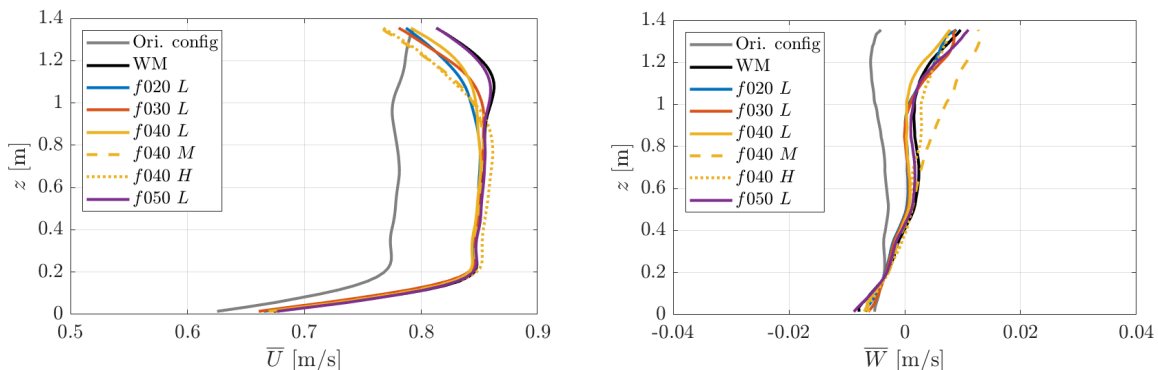


Figure 4: Mean stream-wise velocity  $\overline{U}(z)$  (left) and mean vertical velocity  $\overline{W}(z)$  (right).

To characterise the periodic flow caused by waves, the waves orbital velocity  $U_{orb}$  is calculated from PIV measurements. The case  $f040H$ , which has the higher wave amplitude, has the larger orbital-velocity, up to  $\approx 16\%$  of  $\overline{U}$ . For every single studied

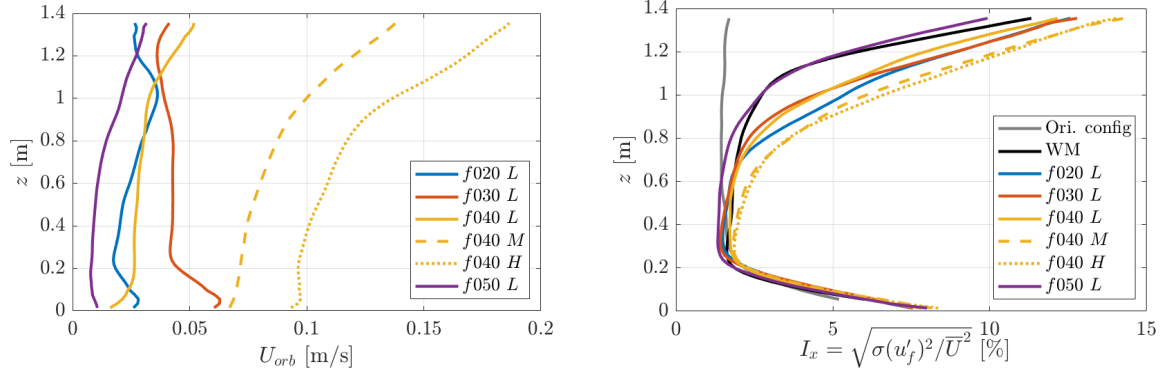


Figure 5: Left: Turbulent intensity  $I_x(z)$  in the stream-wise direction  $x$  at  $(x, y) = (0, 0)$  m.  $I_x$  has been calculated with  $u_f'(x, y, z, t)$  which is  $u'(x, y, z, t)$  filtered at the wave frequency to look at the velocity fluctuations only due to turbulence. Right: Orbital-velocity  $U_{orb}(z)$  in the stream-wise direction at  $(x, y) = (0, 0)$  m.

case, the lower the frequency and the higher the wave amplitude, the higher the orbital-velocity, especially in the bottom part of the tank.

For the six wave conditions tested in this study (opposing a current at 0.8 m/s), four cases have comparable average wave amplitudes and three cases have the same wave frequency. To analyse the impact of these surface waves on the cylinder wake, two reference cases are used : one with the wave-maker and absorber modifying the velocity profile and the turbulence (WM case), and another being the flume tank in its original configuration. In the bottom part of the tank, the wave and WM cases are responsible for an increase of  $\approx 6$  cm/s and a slight increase of the turbulent intensity, 1% higher than when the tank is in its original configuration. Velocity periodic fluctuation amplitude  $U_{orb}$  is high for low frequency and high amplitude waves.

### III – Wave effects on the flow statistics in the wake

In this section, the effects of surface waves propagating against the current on the cylinder wake are investigated. The focus is first made on the effects of frequency  $f_h$  at a fixed wave height and then on the effects of wave amplitude  $\overline{A_{O1}}$  at a fixed frequency.

#### III – 1 Effects of wave frequency $f_h$

In order to study wave frequency  $f_h$  effects on the cylinder wake, the four wave cases with low amplitudes are compared to the WM case (and not to the Original case to focus on waves effects only). Fig. 6 presents maps of the mean velocity components  $\overline{U}$  and  $\overline{W}$ , the turbulent kinetic energy  $k_{2D} = \frac{1}{2}(\overline{u'^2} + \overline{w'^2})$  and the average Reynolds shear stress  $\tau_{u'w'} = \overline{u'w'}$ . In the five cases, the cylinder wake is structured identically, with a recirculation zone (delimited by the dashed line) separated from the outer region (marked by a continuous line) by a highly sheared region, as stated in [5]. A strong upward movement is located above the upper-left corner of the cylinder, with the water bypassing the obstacle. Then a downward movement appears around  $x = 1$  m downstream the cylinder, in agreement with the end of the recirculation zone. In addition,  $k_{2D}$  and  $\tau_{u'w'}$  highlighted the most turbulent region of the cylinder wake, that is started from the upper face of the cylinder and follows the sheared region. Downstream, the wake tends to head toward the surface.

On the covered range of  $f_h$ , low frequency waves seem to have a greater impact on the cylinder wake behaviour than high frequency waves. Indeed, for  $f020L$  and  $f030L$ , turbulent kinetic energy  $k_{2D}$  and Reynolds shear stress  $\tau_{u'w'}$  are far more intense than for the higher frequencies, as shown by  $k_{2D}$  profiles in Fig. 8 (centre and right). Looking at  $k_{2D}$  profiles at  $x = 1.0$  m,  $f020L$  is  $\approx 25\%$  higher than the other cases. Moreover, low frequency waves induce a thickening of the wake compared to WM case as shown by Fig. 8 (left). This is due to a reduction of the recirculation zone and a stronger upward movement of the wake.

To sum up, while  $f040L$  and  $f050L$  do not display significant differences with the WM,  $f030L$  and especially  $f020L$  have a strong effect on the cylinder wake development.

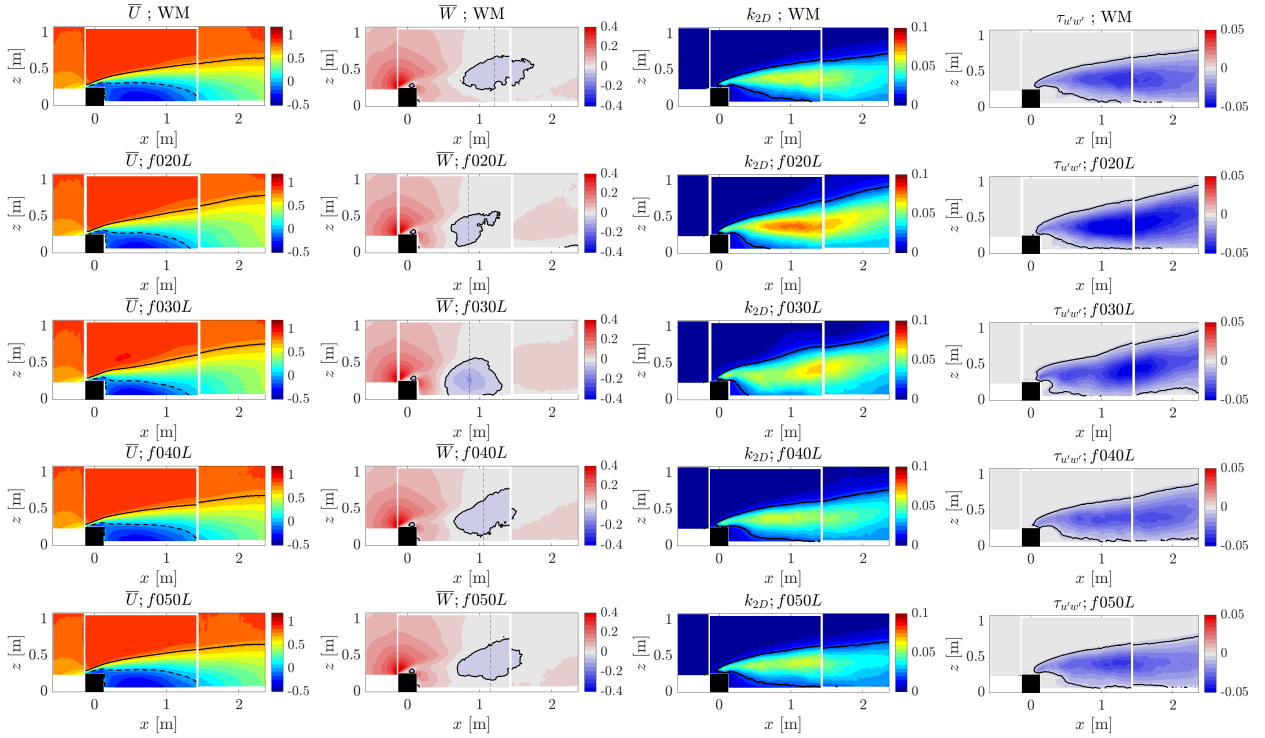


Figure 6:  $\bar{U}$  (m/s),  $\bar{W}$  (m/s),  $k_{2D}$  ( $m^2/s^2$ ) and  $\tau_{u'w'}$  ( $m^2/s^2$ ) colormaps of the cylinder wake. Cases from top to bottom: WM,  $f020L$ ,  $f030L$ ,  $f040L$  and  $f050L$ . On  $\bar{U}$  maps: continuous lines  $\Leftrightarrow \bar{U} = 0.9 \times U_\infty$  & dashed lines  $\Leftrightarrow \bar{U} \leq 0$  m/s. On  $\bar{W}$  maps : continuous lines  $\Leftrightarrow \bar{W} \leq 0$  m/s. On  $\tau_{u'w'}$ : continuous lines  $\Leftrightarrow |\tau_{u'w'}/U_\infty^2| = 0.02$ .

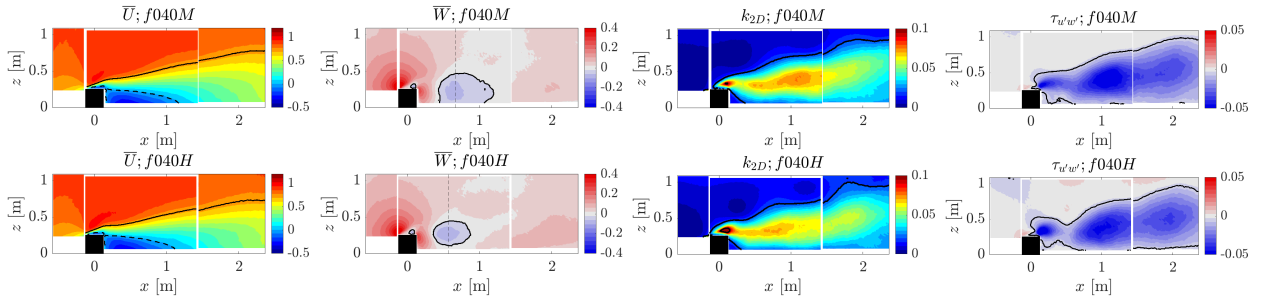


Figure 7:  $\bar{U}$  (m/s),  $\bar{W}$  (m/s),  $k_{2D}$  ( $m^2/s^2$ ) and  $\tau_{u'w'}$  ( $m^2/s^2$ ) colormaps of the cylinder wake. Cases from top to bottom:  $f040M$  and  $f040H$ . On  $\bar{U}$  maps: continuous lines  $\Leftrightarrow \bar{U} = 0.9 \times U_\infty$  & dashed lines  $\Leftrightarrow \bar{U} \leq 0$  m/s. On  $\bar{W}$  maps : continuous lines  $\Leftrightarrow \bar{W} \leq 0$  m/s. On  $\tau_{u'w'}$ : continuous lines  $\Leftrightarrow |\tau_{u'w'}/U_\infty^2| = 0.02$ .

As in [7], low frequency waves seem to be more impactful, contrary to what has been found in [11].

### III – 2 Effects of the wave height

To understand the influence of the wave amplitude on the cylinder wake, the focus is made on the cases WM,  $f040L$ ,  $f040M$  and  $f040H$ . The Fig. 7 presents colormaps of  $\overline{U}$ ,  $\overline{W}$ ,  $k_{2D}$  and  $\tau_{u'w'}$  (as in Fig. 6) for  $f040M$  and  $f040H$ . As expected, the structure of the wake (previously described) is preserved. As for  $f020L$  and  $f030L$ , when waves are high, the recirculation zone is significantly reduced (Fig. 8 left). This makes the downward movement area moving closer to the cylinder and becoming more intense. Levels of  $k_{2D}$  and  $\tau_{u'w'}$  are higher for  $f040M$  and  $f040H$  than for  $f040L$  and WM, especially on top of the cylinder and around  $x = 1$  m in the sheared layer (see Fig. 8 centre and right). Moreover, for the high waves, a deformation of the wake is noticeable on  $k_{2D}$  and  $\tau$  maps. The wake limit is no longer straight and presents bumps around  $x = 1$  m and  $x = 2$  m.

To sum up, at  $f_h = 0.406$  Hz, the case with medium amplitude  $f040M$  is the one having the greatest impact on the cylinder wake. The shape and energy content are strongly modified. When waves are higher, those modifications are slightly less important.

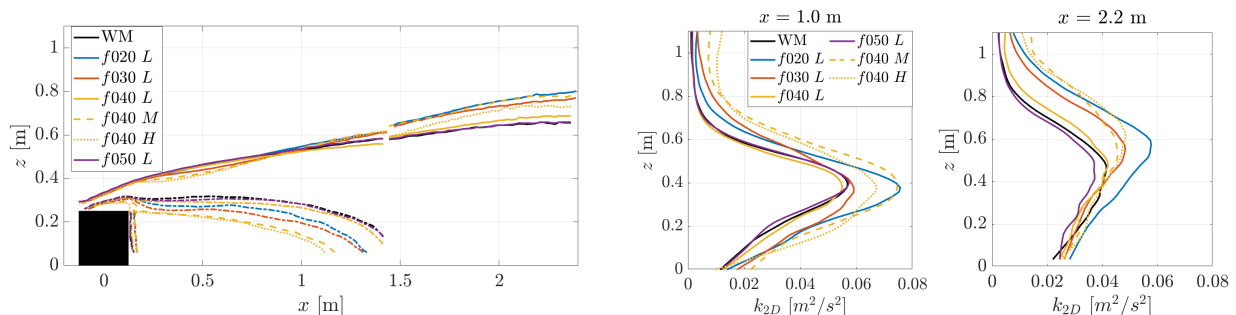


Figure 8: Left: Continuous lines correspond to  $\overline{U} = 0.9 \times U_\infty$ . Dashed lines correspond to  $\overline{U} \leq 0$  m/s Centre and right:  $k_{2D}$  profiles at  $x = 1.0$  m and  $x = 2.2$  m.

From the Fig. 8, the cases with high amplitude  $f040M$  and  $f040H$  impact the recirculation zone by diminishing its size and modify the wake shape, when the cases with a low frequency  $f020L$  and  $f030L$  rather induce a more important wake rise compared to the other cases.

## IV – Vortex shedding frequency shift

### IV – 1 Wave frequency effects

After studying the effects of waves propagating against current on the mean and turbulent quantities in the wake, the spectral content of the flow is studied using the Power Spectral Density (PSD) maps of the fluctuating streamwise velocity component  $u'$ , as introduced in [6]. In Fig. 9, PSD maps are done for all  $z$  at four fixed  $x$ -positions :  $x = 0.0$  m,  $0.4$  m,  $1.4$  m and  $2.4$  m. On each map,  $f_h$  is marked by the yellow dashed line.

On the figure, the left column presents the PSD maps of the flow without the cylinder, made with PIV planes used in the characterisation (section II – 3). The peak at  $f_h$  is visible for  $f030L$  and slightly for  $f020L$  and  $f040L$ . This is in agreement with the  $U_{orb}$

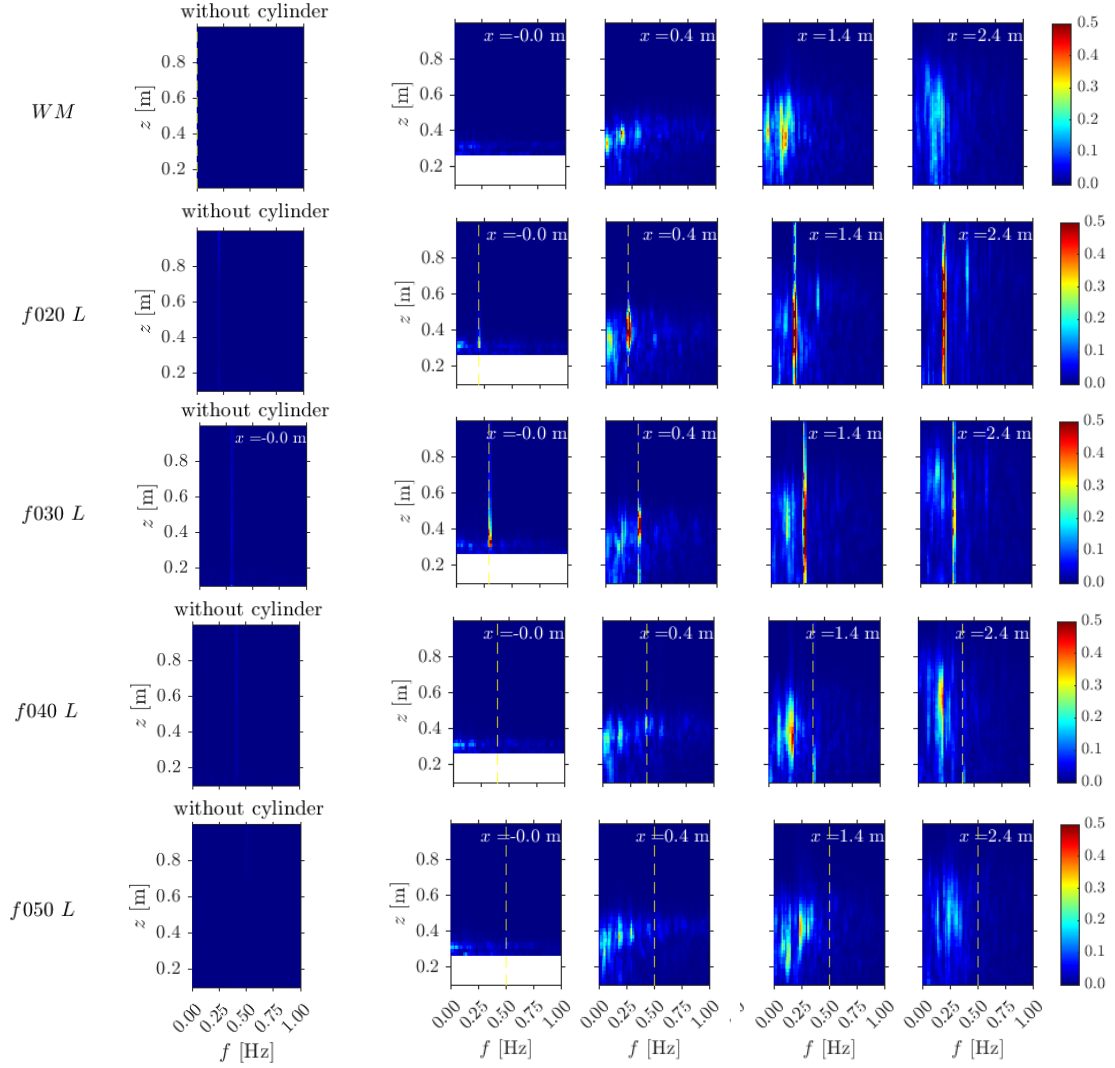


Figure 9: PSD maps of  $u'$  at 4 selected  $x$ -positions in the cylinder wake. The  $x$ -coordinate is indicated on top of each  $(f, z)$  maps. The left column corresponds to maps done without the cylinder. The yellow dashed line corresponds to the wave frequency  $f_h$  for each case.

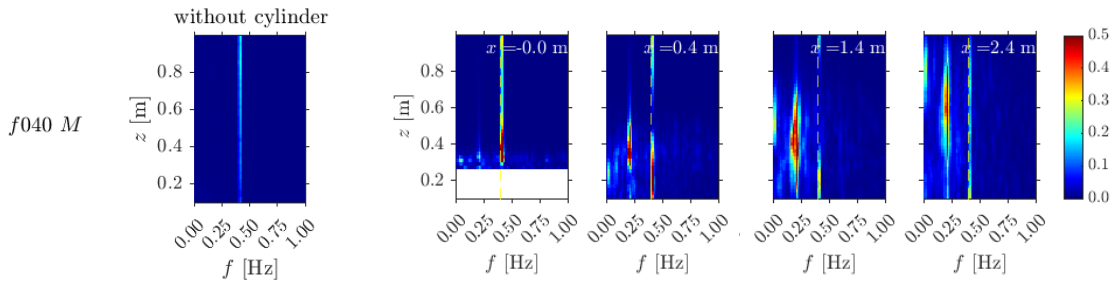


Figure 10: PSD maps of  $u'$  at 4 selected  $x$ -positions in the cylinder wake. The  $x$ -coordinate is indicated on top of each  $(f, z)$  maps. The left column corresponds to maps obtained without the cylinder. The yellow dashed line corresponds to the wave frequency  $f_h$  for each case.

profiles in II – 3, but also with the small modifications of the wake and the recirculation zones observed for  $f040L$  and  $f050L$ .

On the PSD maps with the cylinder (on the right side of the figure), the WM case shows

a peak at  $f \approx 0.25$  Hz. As described in [5], this is the signature of large-scale periodic structures shed by the cylinder towards the surface. This vortex shedding frequency is named  $f_{vort}$  in the following. Even if the wave signature is low without the cylinder, there is an interaction between waves and vortices. For  $f020L$  and  $f030L$ , the  $f_{vort}$  peak shifts on  $f_h$  due to their close values. Shifted peaks are thinner in frequency and are really more intense than in the WM case. In the  $f040L$  and  $f050L$  cases, there is no shift phenomenon. For  $f020L$  and  $f030L$ , the shifted peak is marked on a higher height range. A lower peak around  $z = 0.8$  m is present at  $2f_h = 0.4$  Hz for  $f020L$  and at  $f_h/2 = 0.15$  Hz for  $f030L$ . Thus, the spectral analysis shows that  $f020L$  and  $f030L$  wave cases deeply modify the way vortex generation/development take place.

#### IV – 2 Wave height effects

The same PSD maps are plotted for the case  $f040M$  and are presented in Fig. 10. The case  $f040H$  is not shown here as it behaves exactly in the same way. First looking at the characterisation cases, the peak at  $f_h$  intensifies as the wave height increases (as expected with Fig. 5). In  $f040M$  and  $f040H$  cases, the peak at  $f_{vort}$  related to vortex shedding is observed at 0.20 Hz instead of  $\approx 0.25$  Hz. It is shifted to  $f_{vort} \approx f_h/2$ . It gets more intense and concentrated with the increase of the wave amplitude. Moreover, the  $f_{vort}$  peak is higher (in the  $z$  direction) in the  $f040M$  and  $f040H$  cases than in the WM and small wave amplitude cases.

In addition, varying the amplitude does not generate a new component in the flow, but it concentrates the vortex component into a single intense peak. On the  $f040L$  and WM, this peak is wider in frequency and less intense than for the higher wave amplitudes. A high wave amplitude thus focuses the large vortex shedding peak around one very energetic peak frequency. According to the observations, vortex shedding is present in the cylinder wake and seems to be greatly influenced by wave presence. If waves are high enough, the vortex shedding frequency is modified and becomes extremely regular. Here, an event happens every  $1/\frac{f_h}{2}$  s, with  $f_h = 0.40$  Hz, that is to say almost every 5 s.

#### IV – 3 Vortex visualisation

To study more precisely how the vortex shedding is modified by the surface waves, phase average at the vortex shedding frequency  $f_{vort}$  is performed. The phase averages are linked to the surface elevation  $\eta_A$  above the cylinder. Based on the previous sections and results, five cases are compared : WM,  $f020L$ ,  $f030L$ ,  $f040L$  and  $f040M$ . Four instants of the phase are plotted for the case  $f020L$  in Fig. 11, corresponding to  $\varphi = 0; \frac{\pi}{2}; \pi; \frac{3\pi}{2}$ , with  $\varphi = 0$  when the crest of the wave is on top of the cylinder. The plotted vectors represent the fluctuating-velocity components  $u'$  and  $w'$ . The same scale factor is applied to every single vector for the whole section (Fig. 11 and Fig. 12).

In the Fig. 11 ( $f020L$ ), huge vortices appear in the wake of the cylinder. They emerge in the recirculation region, then are shed and follow the flow while heading towards the surface. At  $x = 2.0$  m, the vortex centre reaches  $z = 0.75$  m. To compare, Fig. 12 displays phase averaged velocity vectors maps for WM,  $f030L$ ,  $f040L$  and  $f040M$  cases when  $\varphi = 0$ . Cases WM and  $f040L$  are similar and do not display well marked and intense vortices. Vortices go toward the surface more slowly: their centre reaching  $z = 0.60$  m when passing by  $x = 2.0$  m.

In a nutshell, lower frequencies like  $f020L$  govern the generation of vortices, mainly explained by the closeness between wave frequency and vortex frequency signature. When

$f_h$  is higher without an increase of the wave amplitude, the wave effects are then less marked due to the gap between  $f_h$  and  $f_{vort}$ . If the amplitude grows, even if the wave frequency is high, the waves drive the vortex shedding. To go deeper, a further step will consist in the description of the vortices size and then comparing the impact of the wave conditions on it.

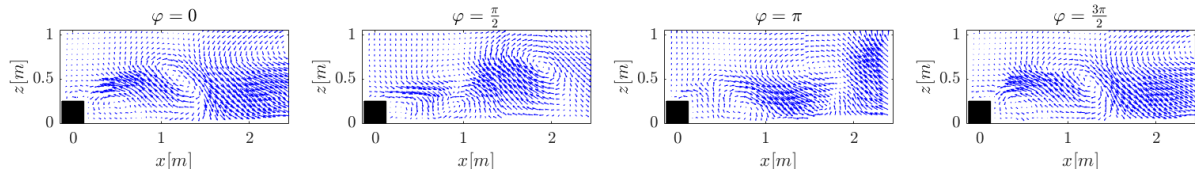


Figure 11: Fluctuating velocity components phase averages at the vortex signature frequency for the case  $f020L$ . The plots correspond to 4 different instants over the phase (from left to right :  $0$ ,  $\frac{\pi}{2}$ ,  $\pi$  and  $\frac{3\pi}{2}$  of the phase).

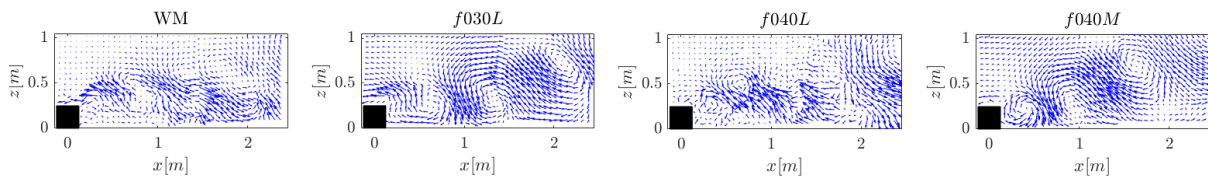


Figure 12: Fluctuating velocity components phase averaged at the vortex signature frequency for the cases WM (left),  $f030L$  (middle-left),  $f040L$  (middle-right) and  $f040M$  (right).

## V – Conclusion

In this paper, the effects of six wave cases propagating against current on the wake of a large bathymetric obstacle are investigated. First, wave cases have been characterised and compared to the reference case, with the wave-maker parked, the damping beach set in position and the only current flow. No profile changes of  $\bar{U}$ ,  $\bar{W}$  and  $I_x$  appeared. Orbital velocity profiles showed that, the higher the wave amplitude and the lower the wave frequency, the greater the impact on the entire water column.

Then, the wave effects on the obstacle wake have been highlighted using mean velocity, turbulent kinetic energy and Reynolds shear stress colormaps. It has been shown that at the same wave amplitude, low frequency waves have greater effects on the cylinder wake than high frequency waves. High amplitudes strengthen the impact of waves on the wake, modifying its energy level but also its shape.

PSD maps displayed the vortex shedding signature of the cylinder. For the low frequency waves, the vortex shedding peak shifts to the wave frequency, which results in a very intense peak. It explains the strong impact of low frequencies on the wake and the generation of very energetic vortices, as presented through the phase average maps. For the fixed-frequency cases, wave and vortex peaks remain separated. However, the vortex shedding peak shifts to a multiple of the wave frequency and becomes more intense and focused.

Finally, the lowest frequencies and the highest amplitudes are the most impacting waves, considerably modifying the cylinder wake intensity and shape. Those interactions

result in vortex shedding, which are amplified for some wave cases. One may wonder about the results that would be obtained for a  $f020H$  case, the lower frequency case with a higher amplitude. As this case is not feasible in the flume tank, it would be interesting to study it numerically. It would likely have a great impact on the cylinder wake and the vortices. Other processing tools will be developed in order to quantify the phenomena energetically, especially by studying the efforts applied to the cylinder for all cases. Differences between waves against current, following current and without current will then be investigated.

## References

- [1] K. Barman, K. Debnath, and B. S. Mazumder. Turbulence between two inline hemispherical obstacles under wave-current interactions. *Advances in Water Resources*, 88:32–52, 2016.
- [2] I. Brevik and A. Bjørn. Flume experiment on waves and currents. i. rippled bed. *Coastal Engineering*, 3:149–177, 1979.
- [3] J.-F. Filipot, M. Prevosto, C. Maisondieu, M. Le Boulluec, and J. Thomson. Wave and turbulence measurements at a tidal energy site. *IEEE/OES CWTM*, 2015.
- [4] L. Furgerot, A. Sentchev, and et al. One year of measurements in Ald. Race: preliminary results from database analysis. *Phil. Trans. R. Soc. A*, 378:20190625, 2020.
- [5] M. Ikhennicheu, G. Germain, P. Druault, and B. Gaurier. Exp. study of coherent flow structures past a wall-mounted square cylinder. *Ocean Eng.*, 182:137–146, 2019.
- [6] M. Magnier, P. Druault, and G. Germain. Experimental investigation of upstream cube effects on the wake of a wall-mounted cylinder: Wake rising reduction, TKE budget and flow organization. *EJM, B/Fluids*, 87:92–102, 2021.
- [7] M. Magnier, B. Gaurier, G. Germain, and P. Druault. Analysis of the wake of a wide bottom-mounted obstacle in presence of surface wave following tidal current. In *Proceedings of the 5th International Conf. on Renewable Energies Offshore*, volume 10 of *Marine Tech. and Ocean Eng. Series*, pages 151–160, 2023.
- [8] P. Mercier, M. Ikhennicheu, S. Guillou, and et. al. The merging of Kelvin–Helmholtz vortices into large coherent flow structures in a high Reynolds number flow past a wall-mounted square cylinder. *Ocean Eng.*, 204:107274, 2020.
- [9] V. Rey, J. Charland, and J. Touboul. Wave-current interaction in the presence of a three-dimensional bathymetry: Deep water wave focusing in opposing current conditions. *Physics of Fluids*, 26(9), 2014.
- [10] S. Roy, K. Debnath, and B. S. Mazumder. Distribution of eddy scales for wave current combined flow. *Applied Ocean Research*, 63:170–183, 2017.
- [11] S. Roy, S. S. Samantaray, and K. Debnath. Study of turbulent eddies for wave against current. *Ocean Engineering*, 150(November 2017):176–193, 2018.
- [12] X. Zhang, R. Simons, J. Zheng, and C. Zhang. A review of the state of research on wave-current interaction in nearshore areas. *Ocean Engineering*, 243:110202, 2022.